Chapter 5 Graphene-zinc oxide hybrid nanolubricants under various test conditions

This chapter explores the development, characterization, and performance evaluation of a novel composite material a hybrid of graphene oxide (GO) sheets and zinc oxide (ZnO) spheres. The synthesis process involved functionalization of ZnO spheres with 3-aminopropyltriethoxysilane (APTES) and attaching GO sheets to prepare a stable and robust hybrid structure AZnOGO*. To confirm the material's chemical functionalities, Fourier Transform Infrared Spectroscopy (FTIR) and Raman spectroscopy were employed, while Transmission Electron Microscopy (TEM) provided insights into its morphology.*

The primary focus of this chapter is on evaluating the tribological performance of hybrid lubricants formulated with the synthesized composite as an additive. The study carefully examines how critical operational parameters such as load, temperature, particle concentration, and sliding speed affect the coefficient of friction (COF) under flooded lubrication conditions. A key highlight of this work is to emphasis the interactions between these parameters, an aspect often overlooked due to the complexities involved in tribological testings. Using Analysis of Variance (ANOVA), the relative importance of each parameter and their combined effects were assessed, offering valuable insights. Additionally, Response Surface Methodology (RSM) was applied to develop predictive models for estimating COF under varying conditions with the help of design expert software. Beyond its role as a lubricant additive, the hybrid material exhibits promising thermal and electrical properties, making it a candidate for broader applications, such as in the fabrication of micro- and nano-scale devices. This chapter not only demonstrates the multifaceted potential of GO-ZnO hybrid nanocomposites but also lays a strong

foundation for their utilization in advanced engineering systems. By bridging material science and tribological engineering, this work underscores the innovative possibilities for hybrid nanomaterials in addressing contemporary challenges.

5.1. Characterization of particles

5.1.1. XRD analysis

The X-ray diffraction (XRD) analysis was performed to explore the crystalline structure and identify the phases present in the materials being studied. By comparing the diffraction patterns of zinc oxide (ZnO) with the standard reference data (JCPDS 36-1451), we were able to match the characteristic peaks to specific crystallographic planes. These peaks reflect the angles and intensities associated with the crystal structure of ZnO.

Figure 5.1 shows the XRD patterns of both ZnO and the AZnOGO composite material. This comparison highlights the similarities and differences in their structures. The results reveal that the key peaks seen in ZnO corresponding to specific planes listed in the JCPDS file are also present in the AZnOGO composite. This confirms that the crystalline structure of ZnO remains intact within the hybrid material.

One noticeable difference, however, is the appearance of an additional peak at the (002) plane in the hybrid AZnOGO, which is not seen in pure ZnO. This peak is attributed to graphene oxide (GO), as also noted in the literature [101]. The incorporation of GO adds its own distinct structural features, such as the (002) peak, which corresponds to the layered arrangement of graphene oxide. The retention of ZnO's characteristic peaks in the hybrid material suggests that its crystalline structure was maintained throughout the synthesis process.

Meanwhile, the presence of the (002) peak confirms that graphene oxide was successfully integrated into the composite. This combination of ZnO and GO could potentially

enhance the material's properties, such as its mechanical strength, thermal stability, or electrical conductivity, depending on how the hybrid is intended to be used.

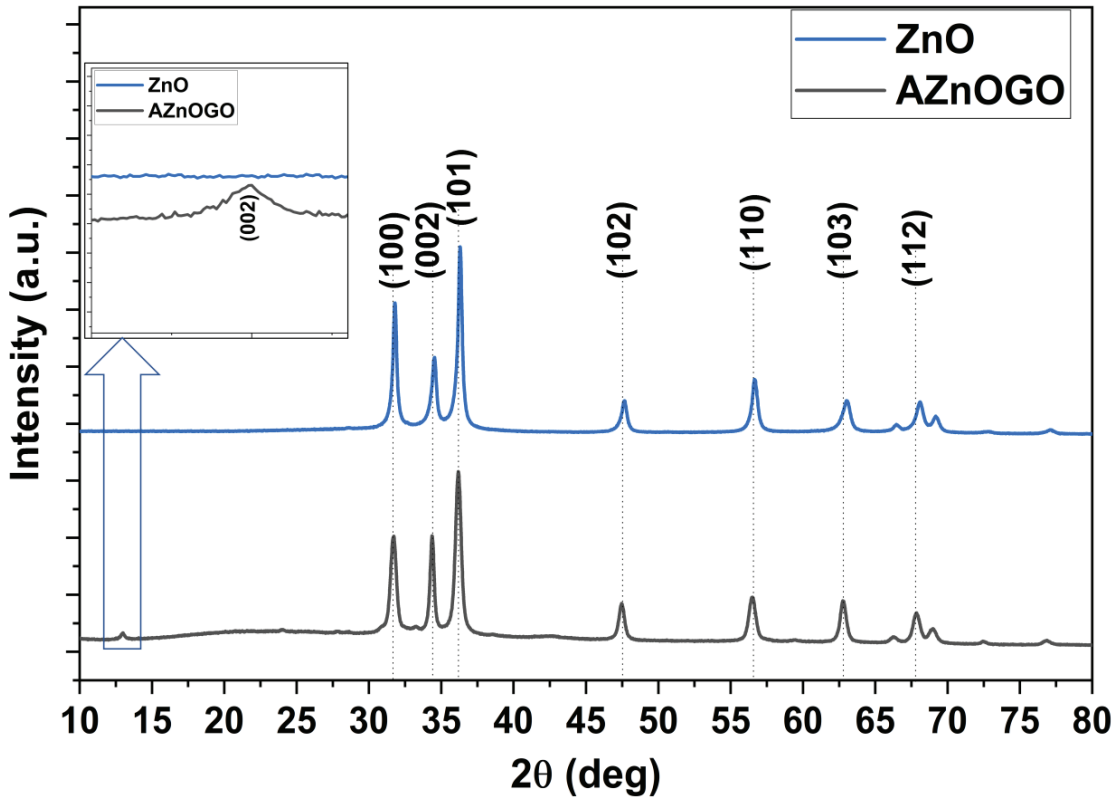

Figure 5.1 XRD results of hybrid particles

5.1.2. FTIR results of hybrid nano additives

The functionalization of ZnO and graphene oxide with APTES was confirmed through FTIR spectroscopy, which measures the transmittance associated with bond vibrations. The FTIR spectrum (Figure 5.2) highlights key vibrational peaks, revealing the chemical modifications.

A strong and distinct peak at 3411 cm^{-1} corresponds to the hydroxyl group (O-H), likely due to the presence of surface hydroxyls and adsorbed water molecules [102]. In the case of APTES-functionalized ZnO (AZnO), this peak shifts slightly to 3497 cm^{-1}, indicating hydroxyl groups are present on the ZnO surface post-functionalization. Additionally, a

vibrational peak at 437 cm^{-1}, associated with the Zn-O bond [103], is also visible in the AZnOGO hybrid at a slightly shifted position of 437.5 cm^{-1}.

Further confirmation of functionalization deduces from the Zn-O-Si bond stretching vibration, which is observed at 920 cm^{-1} [104,105]. These vibrational peaks confirm that the APTES molecule has successfully bonded with the ZnO structure. Another notable feature is the peak at 1105 cm^{-1} in the AZnOGO spectrum, which corresponds to the vibrational mode of the C-N bond. This provides clear evidence that the APTES-functionalized ZnO has been successfully incorporated with the graphene oxide surface, forming the hybrid material.

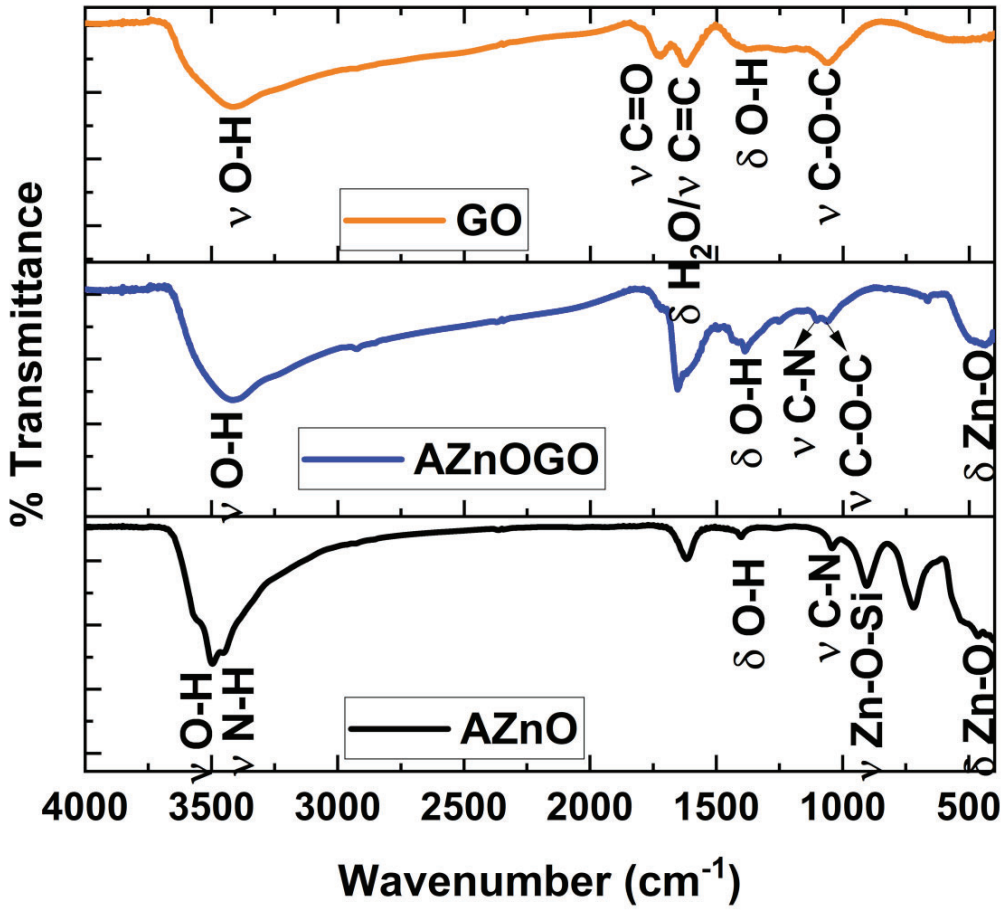

Figure 5.2: FTIR results of hybrid nano additives

5.1.3. Raman spectroscopic results of AZnOGO hybrid

The Raman spectrum of the hybrid material (AZnOGO) as shown in Figure 5.3, reveals key insights into its structural characteristics. Two prominent peaks, known as the D and G bands, were observed at 1357 and 1602 cm^{-1}, respectively. The D band is linked to defects in the graphene structure, which arise due to the incorporation of oxygen-containing functional groups, structural defects, and edges in the graphitic skeleton of GO. On the other hand, the G band is associated with the in-plane vibration of sp2-hybridized carbon atoms and represents the scattering of the E2g mode in the first order.[106]

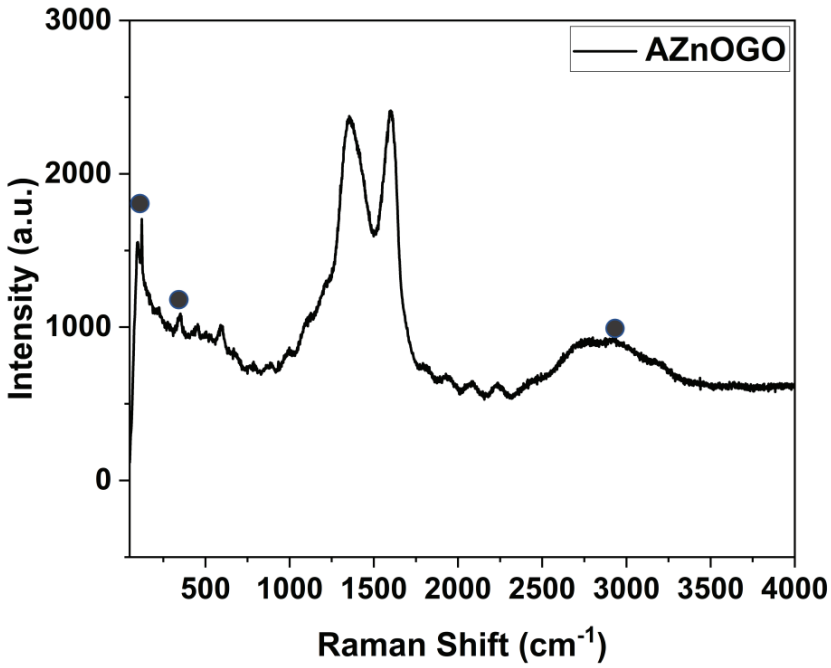

Figure 5.3: Raman spectrum of AZnOGO hybrid

One of the most important indicators of graphene's structural orderliness is the ratio of the intensities of the D and G bands (I_D/I_G ratio). A ratio greater than one, typically reflects increased imperfections, voids, and structural disorder within graphene oxide [107]. However, in the case of the hybrid AZnOGO, the ID/IG ratio is measured at 0.978, which suggests a noticeable reduction in the level of disorder after modification. This

improvement implies a better-quality graphene oxide structure, with fewer defects and enhanced material integrity.

Additionally, the Raman spectrum displays characteristic peaks at 330, 435, and 550 cm^{-1}, which can be attributed to the presence of zinc oxide within the hybrid. Overall, the Raman analysis highlights the structural refinement of graphene oxide in the hybrid material, pointing toward the improved quality and potential functionality of the AZnOGO composite.

5.1.4. Morphological studies

The TEM images provide valuable insights into the morphology of the materials under study. As shown in Figure 5.4(a), the ZnO particles exhibit a distinct spherical shape with an average size of ~24 nm. This uniformity in size and shape highlights the well-controlled synthesis of ZnO. The AZnOGO hybrid is illustrated in Figure 5.4(b), where the spherical ZnO particles can be seen distributed across the surface of the GO sheets. This distribution demonstrates an interaction between the ZnO particles and the GO, with ZnO evenly spread throughout the composite material. Such uniform dispersion is crucial, as it ensures that the properties of both components ZnO and GO are effectively integrated.

One notable observation is the improved dispersion of the hybrid AZnOGO compared to pure graphene. The presence of ZnO particles enhances the stability of the material, particularly in vegetable oil, as the surface of ZnO contributes to reducing agglomeration. This improved stability and dispersion are essential for applications where the material needs to maintain consistent performance in a liquid medium, such as in lubricants or coatings [108]. The TEM images confirm the successful integration of ZnO onto graphene oxide, resulting in a hybrid material with enhanced dispersion and stability, making it more suitable for practical applications.

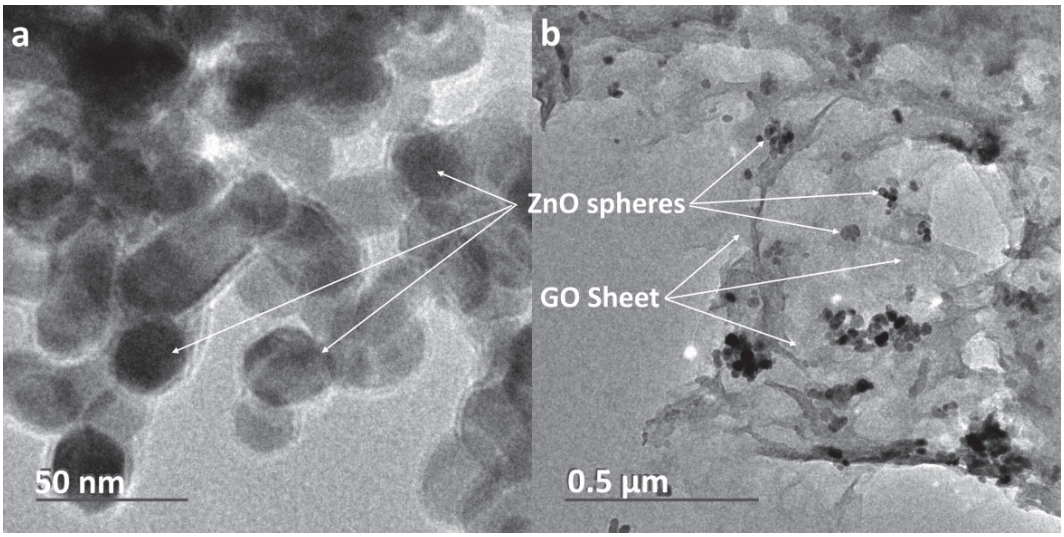

Figure 5.4: TEM images of hybrid nano additives AZnOGO

5.2. Dispersion stability of lubricants

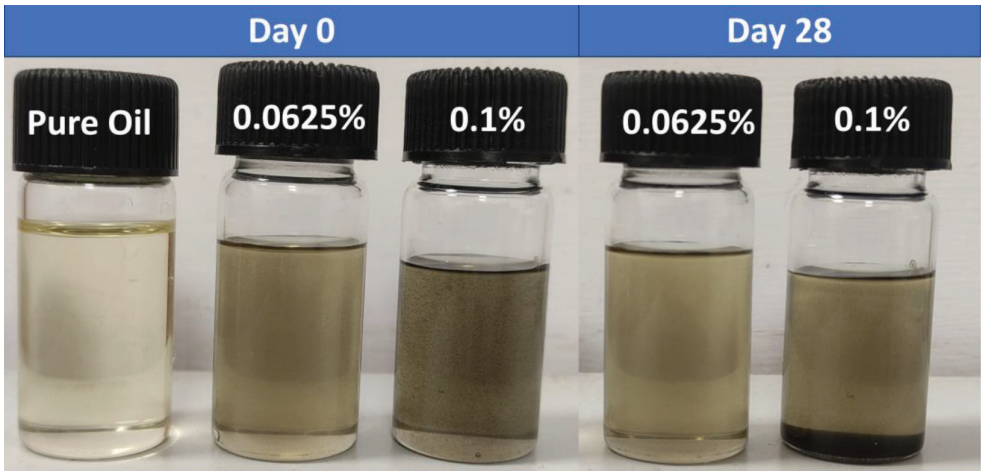

Figure 5.5: Digital images of lubricants mixed with pure castor oil

The AZnOGO hybrid shows good dispersion due to the ZnO nanoparticles. These nanoparticles play a crucial role by making the material more stable and compatible with vegetable oil, the base medium in this case. Zinc oxide has a polar surface that interacts well with the oil's polar components. This prevents clumping and keeps the AZnOGO evenly distributed as depicted in Figure 5.5.

By stabilizing the interface between the GO and the oil, zinc oxide helps the material spread out more uniformly. This improved dispersion not only ensures a more consistent mixture but also boosts the material's performance, especially in terms of thermal and tribological properties. With the graphene layers staying separated and active, the hybrid material can work more effectively within the lubricant.

5.3. Thermophysical properties of lubricants

Table 5.1 summarizes the thermophysical properties of the lubricant before and after the incorporation of hybrid particles, along with their respective units. The results reveal a reduction in viscosity at 30 °C, which is primarily attributed to the presence of residual hexane in the wet cake of the hybrid particles. At temperatures above 70 °C, under standard atmospheric pressure, the hexane component evaporates from the mixture. Beyond this temperature, the differences in viscosity between the hybrid lubricant and pure oil are minimal.

The inclusion of GO sheets in the hybrid lubricant significantly enhances its thermal conductivity and thermal effusivity. This improvement is due to the intrinsic properties of GO, which has a high heat transfer capacity and functions as an effective heat carrier. These characteristics enable the hybrid lubricant to dissipate heat more efficiently, making it well-suited for applications requiring enhanced thermal performance.

Table 5.1 Thermophysical properties of nanolubricants

Properties	Pure Oil	0.1 wt% Hybrid Oil	Unit
Viscosity (at 30 °C)	471.0	458.0	cP
Viscosity (at 75 °C)	40.3	40.2	cP
Specific gravity (at 25 °C)	0.960	0.961	------
Thermal conductivity	0.178	0.203	W/m/K

Thermal Effusivity	262.2	602.9	$Ws^{0.5}/m^2$
Specific heat	0.387	0.793	$MJ/m^3/K$

5.4. Tribological investigation of nano lubricants

Figure 5.6 shows how the coefficient of friction (COF) changes over time for pure castor oil and castor oil mixed with different amounts of hybrid nanolubricants. The test was done using a four-ball tester following ASTM D 4172b standards, which measures how well a lubricant reduces friction between surfaces. Pure castor oil, shown by the black line (Figure 5.6), has the highest friction throughout the test, meaning it doesn't lubricate as effectively as the mixtures with hybrid nanolubricants.

When even a small amount of hybrid nanolubricants (like 0.025 wt%) is added, the friction decreases, as seen in the red line (Figure 5.6). As the concentration of nanoparticles increases, the friction keeps dropping, with the 0.1 wt% mixture (yellow line; Figure 5.6) showing the lowest friction and the best performance, amongst all samples being explored. At the start of the test, there's a run-in period (the first 600 seconds), where friction fluctuates as the system settles, but after that, the friction levels become more stable for all samples.

The results show that adding hybrid nanolubricants significantly improves the lubrication properties of castor oil. This happens because the nanoparticles help to carry the load better and create a thin protective layer that reduces direct contact between surfaces. The higher the concentration of nanoparticles, the more effective the lubrication. This makes hybrid nanolubricants a promising way to enhance the performance of vegetable oils like castor oil for lubricant various applications.

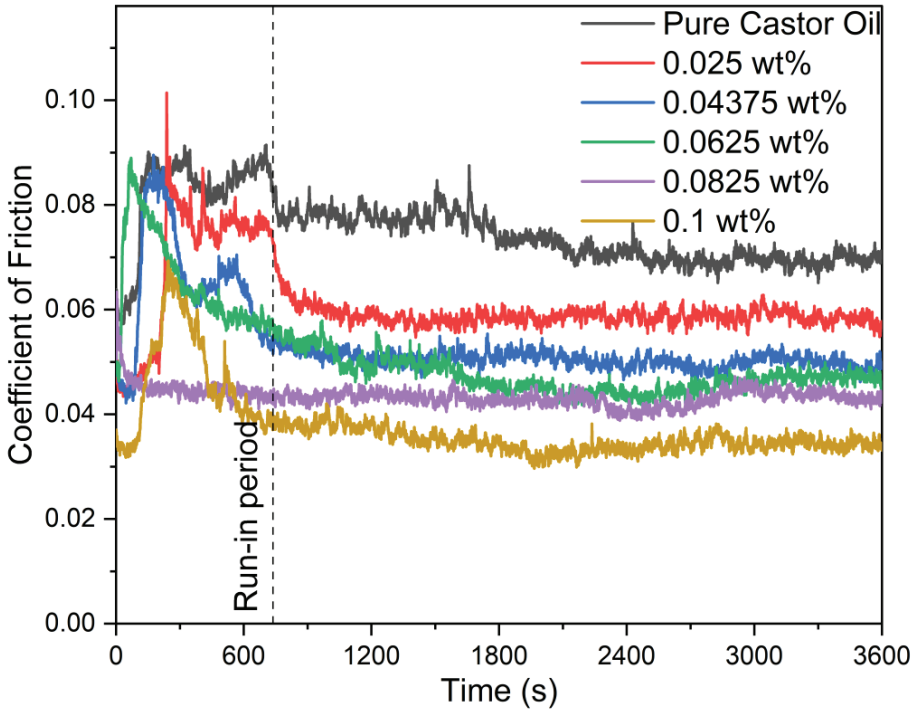

Figure 5.6: Tribological test results as per ASTM D 4172b of different wt% added hybrid additives

5.5. Worn surface analysis of lubricants

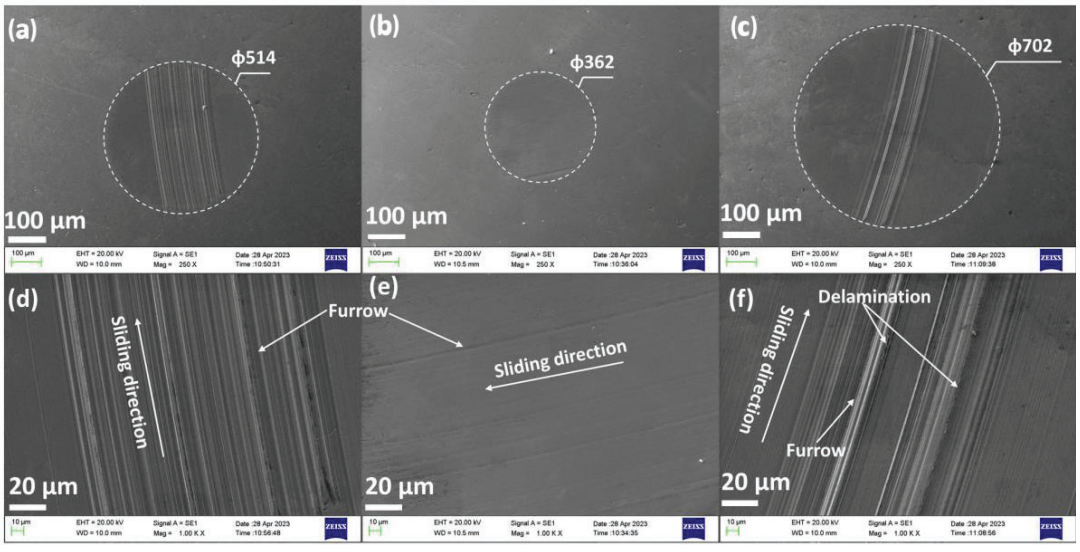

Figure 5.7: Wear scar images of a tested ball subjected to 200 N applied load, 50 °C temperature, and 0.2687 m/s sliding speed for (a, d) 0.025 wt%, (b, e) 0.0625 wt%, and (c, f) 0.1 wt% hybrid lubricant.

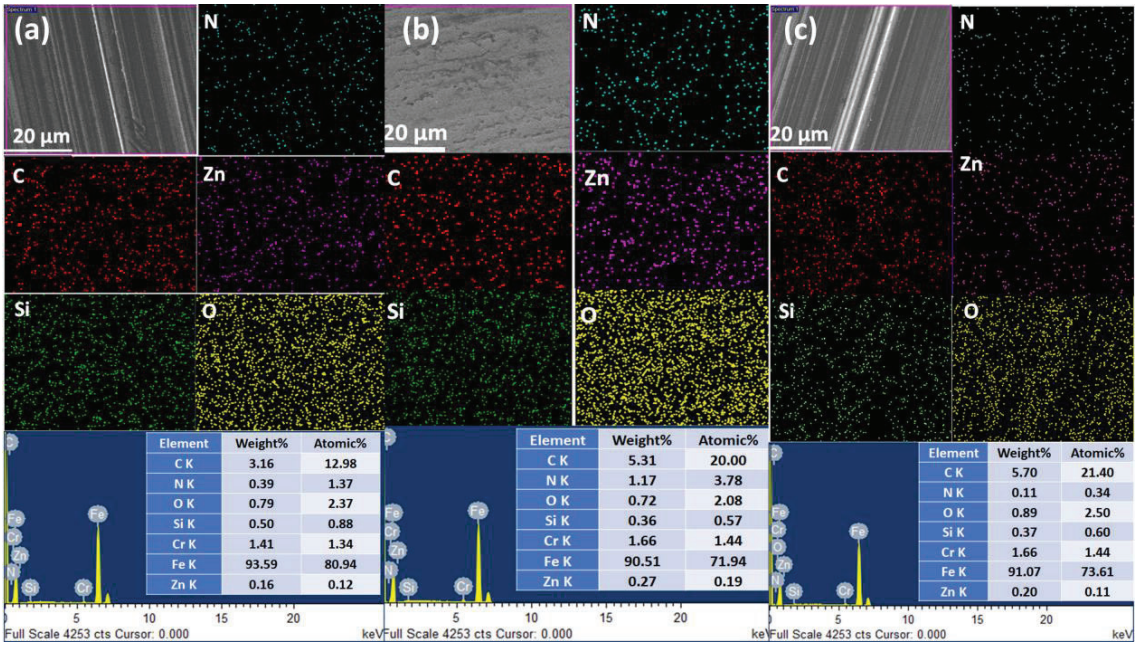

Figure 5.8 EDX mapping of the worn surface of steel balls after tribo-tests using (a) 0.025 wt%, (b) 0.0625 wt%, and (c) 0.1 wt% concentrations of hybrid nanolubricant

The worn balls from the tribological tests were carefully analysed using scanning electron microscopy (SEM) to understand the impact of hybrid nanolubricant (HNL) under varying concentrations. The analysis focused on three key concentration levels low, mid, and high within the test range, as shown in Figure 5.7 (a) to (c). To isolate the effect of the hybrid additive, all other variables were kept identical during the tribo experiments.

One noticeable observation was the presence of furrows on the worn surfaces, which are characteristic of abrasive wear. These furrows were more pronounced at both low and high concentrations of HNL, whereas at medium concentrations, their presence was significantly reduced. Interestingly, when the concentration of HNL was increased to 0.0625 wt%, the surface appeared smoother, with a marked reduction in furrows, suggesting better antiwear performance. However, as the concentration increased further, the wear rate began to rise. This was attributed to the aggressive behavior of zinc oxide

particles in the lubricant, which can lead to more intense interactions with the surface [109].

Figure 5.8 complements this analysis by providing elemental mapping of the worn surfaces, captured at a magnification of 5000x using energy-dispersive X-ray (EDX) analysis. The mapping reveals the composition of the bearing steel AISI 52100, primarily consisting of Fe, C, and Cr, alongside the elemental components of the HNL, including C, N, Si, Zn, and O. The detection of these elements on the worn surfaces suggests that the particles deposit during tribo-performance tests, creating a thin layer. This deposition could be indicative of a self-repairing mechanism, where the nanomaterials fill micro-grooves or defects, potentially reducing further damage and improving surface integrity. This behaviour highlights the multifaceted role of HNL in not only reducing wear but also in contributing to surface restoration during operation.

5.6. Worn surface profile

Figure 5.9 depicts the contour of the worn surface, as well as the associated root mean square roughness of the tested ball, in accordance with the ISO 4287 standard. The graph provides a clear picture of how the surface roughness of worn balls changes with different concentrations of the hybrid nanolubricant (AZnOGO). When pure oil is used, the surface is the roughest, with deep grooves and peaks that result in the highest RMS roughness value, showing significant wear. Adding a small amount of AZnOGO, at 0.025 wt%, leads to a noticeable improvement the surface becomes smoother, and the roughness decreases. This trend continues as the concentration is increased to 0.04375 wt%, with further smoothing of the surface and a lower RMS roughness value.

The best results are seen at 0.0625 wt%, where the surface is at its smoothest, with minimal grooves or irregularities, and the RMS roughness reaches its lowest point. This indicates that the lubricant performs most effectively at this concentration, reducing wear

and creating a more uniform surface. However, when the concentration increases beyond this optimal level, the improvements start to reverse. At 0.08125 wt%, the roughness begins to increase slightly, and at 0.1 wt%, the surface becomes noticeably rougher again, with more pronounced grooves and a higher RMS roughness value. This suggests that too much AZnOGO can actually harm the surface, possibly because the zinc oxide particles become too aggressive, leading to abrasion or particle buildup. In summary, while AZnOGO significantly improves surface smoothness and reduces wear at moderate concentrations, overusing it can lead to the detrimental effect and enhances the wear. The optimal performance of the lubricant is observed at a nanoparticle concentration of 0.0625 wt%, where it demonstrates the most favourable balance between wear reduction and surface smoothness.

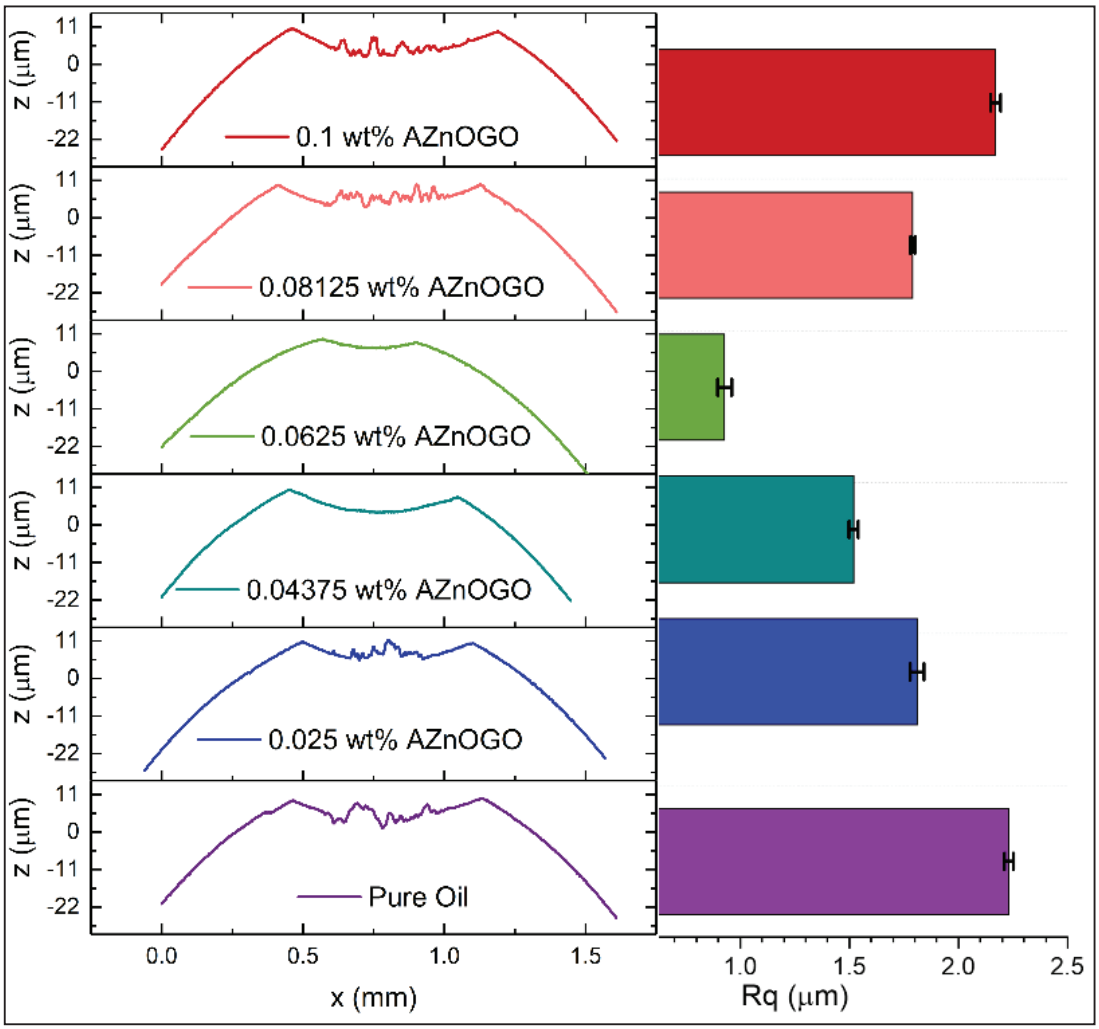

Figure 5.9: Worn surface contour with corresponding RMS roughness (Rq)

5.7. Statistical analysis

5.7.1. Response surface methodology (RSM)

The present study employs a statistical methodology known as Response Surface Methodology (RSM) to analyse the impact of parameter variations on the coefficient of friction observed in tribological tests conducted on a hybrid lubricant. The objective of employing Response Surface Methodology (RSM) is to analyse the effects of the parameter and determine the optimal settings that maximise the performance of the HNL functions. Equation 5.1 presents the comprehensive representation of the output response.

$$Y = f(V_1, V_2, V_3, .. V_n) + N_\varepsilon \qquad [5.1]$$

Where Y is the output response, Vi's are independent variables, often known as natural variables, and N_ε is the variability that is not accounted in f. Variability during measurement can arise due to background noise, measurement error, and the influence of other potential factors that are not taken into account in f. Because interaction between factors is typical in tribological investigations, a 2nd order model is chosen, as indicated in equation 5.2.

$$Y = a_0 + \sum_{i=1}^{n}(a_i v_i) + \sum_{i=1}^{n}(a_{ii} v_i^2) + \sum_{i=1}^{n-1}\sum_{j=i+1}^{n} a_{ij} v_i v_j \qquad [5.2]$$

Where v_i represents the variables or factors, a_o, a_i, a_{ii}, and a_{ij} are the constant and coefficients of the parameters and the interaction terms respectively.

Table 5.2 Factors and levels selected for the study

Factor(code)	Unit	Axial -α	Factorial -1	Centre 0	Factorial 1	Axial +α
Speed (A)	m/s	0.153555	0.21114	0.268725	0.32631	0.383895
Load (B)	N	100	150	200	250	300
Concentration (C)	wt%	0.025	0.04375	0.0625	0.08125	0.1
Temperature (D)	°C	25	37.5	50	62.5	75

Table 5.3 Actual design with output response with run order

Std	Run	A:Speed m/s	B:Load N	C:Concentration wt%	D:Temperature °C	COF
23	1	0.268725	200	0.0625	25	0.07865
19	2	0.268725	100	0.0625	50	0.07612
21	3	0.268725	200	0.025	50	0.085071
16	4	0.32631	250	0.08125	62.5	0.073568
30	5	0.268725	200	0.0625	50	0.07549
12	6	0.32631	250	0.04375	62.5	0.08088
11	7	0.21114	250	0.04375	62.5	0.080102
25	8	0.268725	200	0.0625	50	0.07689
13	9	0.21114	150	0.08125	62.5	0.074251
15	10	0.21114	250	0.08125	62.5	0.07254
2	11	0.32631	150	0.04375	37.5	0.08085
22	12	0.268725	200	0.1	50	0.06847
14	13	0.32631	150	0.08125	62.5	0.07125
5	14	0.21114	150	0.08125	37.5	0.07854
20	15	0.268725	300	0.0625	50	0.07658
3	16	0.21114	250	0.04375	37.5	0.08097
10	17	0.32631	150	0.04375	62.5	0.08057
4	18	0.32631	250	0.04375	37.5	0.08078
29	19	0.268725	200	0.0625	50	0.07654
8	20	0.32631	250	0.08125	37.5	0.071178
26	21	0.268725	200	0.0625	50	0.07547
24	22	0.268725	200	0.0625	75	0.07656
1	23	0.21114	150	0.04375	37.5	0.08097

18	24	0.383895	200	0.0625	50	0.07895
27	25	0.268725	200	0.0625	50	0.07523
17	26	0.153555	200	0.0625	50	0.08064
28	27	0.268725	200	0.0625	50	0.07556
6	28	0.32631	150	0.08125	37.5	0.07121
7	29	0.21114	250	0.08125	37.5	0.07659
9	30	0.21114	150	0.04375	62.5	0.08081

The present investigation examines the influence of factors such as speed, load, particle concentration, and temperature, which are found to have a significant effect on friction. The test has been constructed utilising a randomised central composite design (CCD) comprising five tiers and six repeats of the centre point. Table 5.1 presents the parameters selected for the present study and the corresponding levels at which they were established. Table 5.2 shows the factual design along with the corresponding responses.

Table 5.4 ANOVA for test data with all variables specified.

Source	**Sum of Squares**	**df**	**Mean Square**	**F-value**	**p-value**	
Model	0.0004	14	0.0000	27.74	< 0.0001	significant
A-Speed	0.0000	1	0.0000	12.66	0.0029	
B-Load	3.550E-08	1	3.550E-08	0.0338	0.8566	
C-Concentration	0.0003	1	0.0003	321.37	< 0.0001	
D-Temperature	5.318E-06	1	5.318E-06	5.06	0.0399	
AB	2.971E-06	1	2.971E-06	2.83	0.1133	
AC	0.0000	1	0.0000	13.29	0.0024	
AD	8.435E-06	1	8.435E-06	8.03	0.0126	
BC	5.142E-08	1	5.142E-08	0.0490	0.8279	
BD	3.195E-07	1	3.195E-07	0.3042	0.5894	
CD	1.381E-06	1	1.381E-06	1.31	0.2695	
A^2	0.0000	1	0.0000	21.61	0.0003	
B^2	6.455E-08	1	6.455E-08	0.0615	0.8076	

C^2	6.474E-07	1	6.474E-07	0.6164	0.4446	
D^2	3.600E-06	1	3.600E-06	3.43	0.0839	
Residual	0.0000	15	1.050E-06			
Lack of Fit	0.0000	10	1.346E-06	2.93	0.1238	not significant
Pure Error	2.299E-06	5	4.598E-07			
Cor Total	0.0004	29				

The absence of correlation between factors is of utmost importance since any non-zero correlation between elements might have a negative effect on the accuracy of model prediction. The utilisation of analysis of variance (ANOVA) and F-test is employed to evaluate the suitability of the model. The findings of the relevant test are presented in Table 5.3. A p-value below 0.05 for the model signifies its significance, indicating a reduced likelihood that the null hypothesis is valid. A smaller p-value and a larger F-value are desirable to establish the statistical significance of the model.

Figure 5.10 illustrates the usual residual plot, demonstrating a strong correlation between the equality lines. The comparison between the anticipated and actual data shows a high degree of proximity to the line of equality. The box-cox results indicate that the value closest to one corresponds to the lowest point, suggesting that the model does not require any change. Additionally, the residual versus anticipated plot demonstrates that the dispersion of data points falls within acceptable boundaries. The fit statistics of the model indicate a small difference of less than 0.2 between the predicted R^2 and adjusted R^2. Additionally, the accuracy value and signal-to-noise ratio of 16 are reasonable. These findings suggest that the model is suitable for investigating the design space. Equation 5.3 represents the normalized mathematical model that is generated from the Response Surface Methodology (RSM). Whereas equation 5.4 is the actual model predicted from RSM.

$$Y = 0.0757 - 0.0007A - 0.0038C - 0.0005D + 0.0004AB - 0.0009AC + 0.0007AD - 0.0001BC + 0.0001BD - 0.0003CD + 0.0010A^2 + 0.0001B^2 + 0.0002C^2 + 0.0004D^2 \quad [5.3]$$

Coefficient of friction = 0.12662 - 0.18668(speed) - 5.62767e-05(load) + 5.25741e-02(concentration) - 5.07431e-4(temperature) + 1.4967e-4(speed.load) - 0.86498(speed.concentration) + 1.00868e-3(speed.temperature) - 6.04666e-05(load.concentration) + 2.26100e-07(load.temperature) - 1.2536e-3(concentration.temperature) + 0.27435(speed)^2 + 1.940416e-08(load)^2 + 0.43700(concentration)^2 + 2.31847e-06(temperature^2) [5.4]

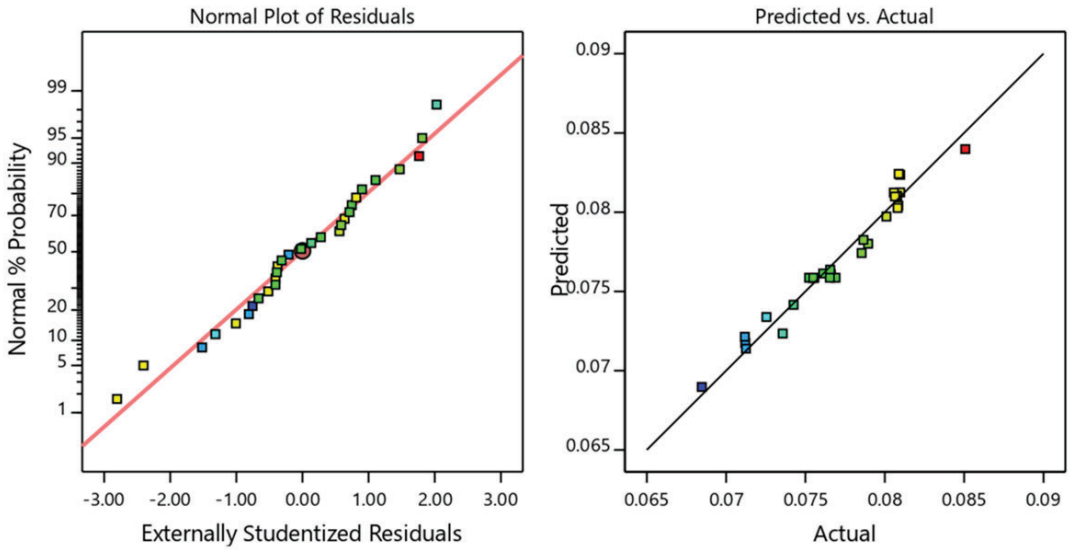

Figure 5.10 Residual plot and predicted vs actual plot with different test data

The negative sign suggests that increasing the parameter will reduce the response. The coefficient of friction decreases as attributes like speed, concentration, and temperature increases. As the speed increases, the lubrication regime changes and boundary region is

at lower speed. As a result, COF falls. The viscosity of the lubricant changes directly as the temperature changes. Shearing between layers becomes easier when viscosity falls, lowering COF. The variation on coefficient of friction by various factor values are enlisted in Figure 5.11. The graph shows the variation in COF considering single factor change neglecting interaction, while the dashed lines represent the 95% confidence interval range. Changes in factors A and C induce the greatest change in COF, as shown in Figure 5.11. This study provides a broad overview of each aspect, which may not be comprehensive enough for a tribological application. Given the observed synergistic relationship between the components, it is imperative to do further investigation into the effects of these factors and their interactions. The outcomes of the interaction are presented in the subsequent section.

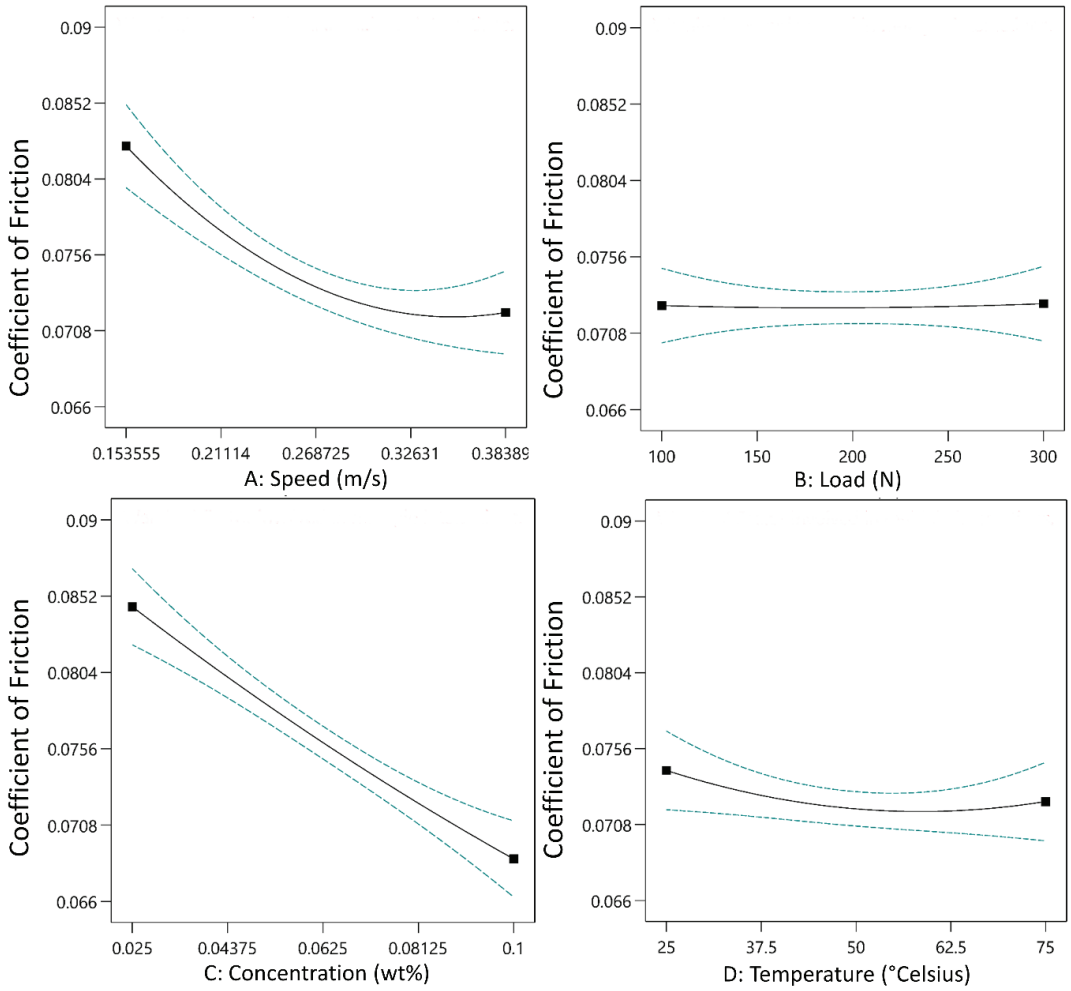

Figure 5.11: Variation on coefficient of friction with respect to factors at different values with 95% confidence interval in dashed line

5.7.2. Individual factors

The study finds that speed, concentration, and temperature significantly influence COF, as seen in Figure 5.11. The COF decreases as speed increases, likely due to changes in lubrication regimes. At higher speeds, the transition from boundary to hydrodynamic lubrication reduces asperity interactions, lowering friction. Similarly, rising temperatures reduce lubricant viscosity, easing shearing between layers and further decreasing COF. Notably, concentration has the most pronounced impact on COF, while load shows a relatively minor effect.

5.7.3. Interaction effects between factors

5.7.4. Load-speed interaction

The interplay between load and speed varies across lubrication regimes is shown in Figure 5.12. According to the Hamrock equation, speed directly influences film thickness, while load impacts the contact area between surface asperities. At lower speeds, COF decreases with increasing load due to asperity deformation and wider contact areas. However, at higher speeds, increasing load results in reduced film thickness, reversing the trend. The COF initially drops with rising speed, reaching a minimum at 0.25 m/s, before increasing due to interlayer shear in the viscous lubricant.

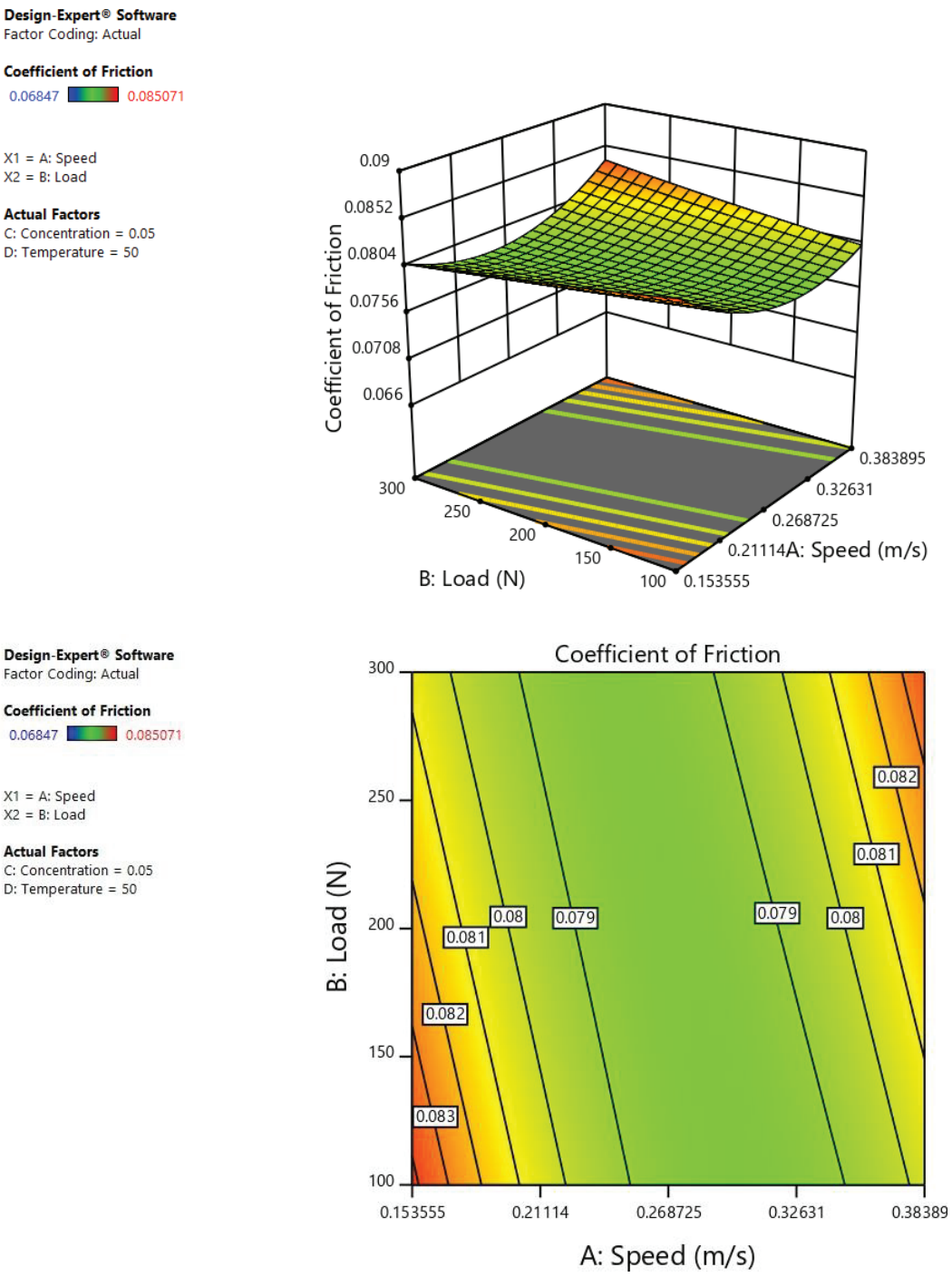

Figure 5.12 Load-speed interaction 3D graph and its contour plot

5.7.5. Load-temperature interaction

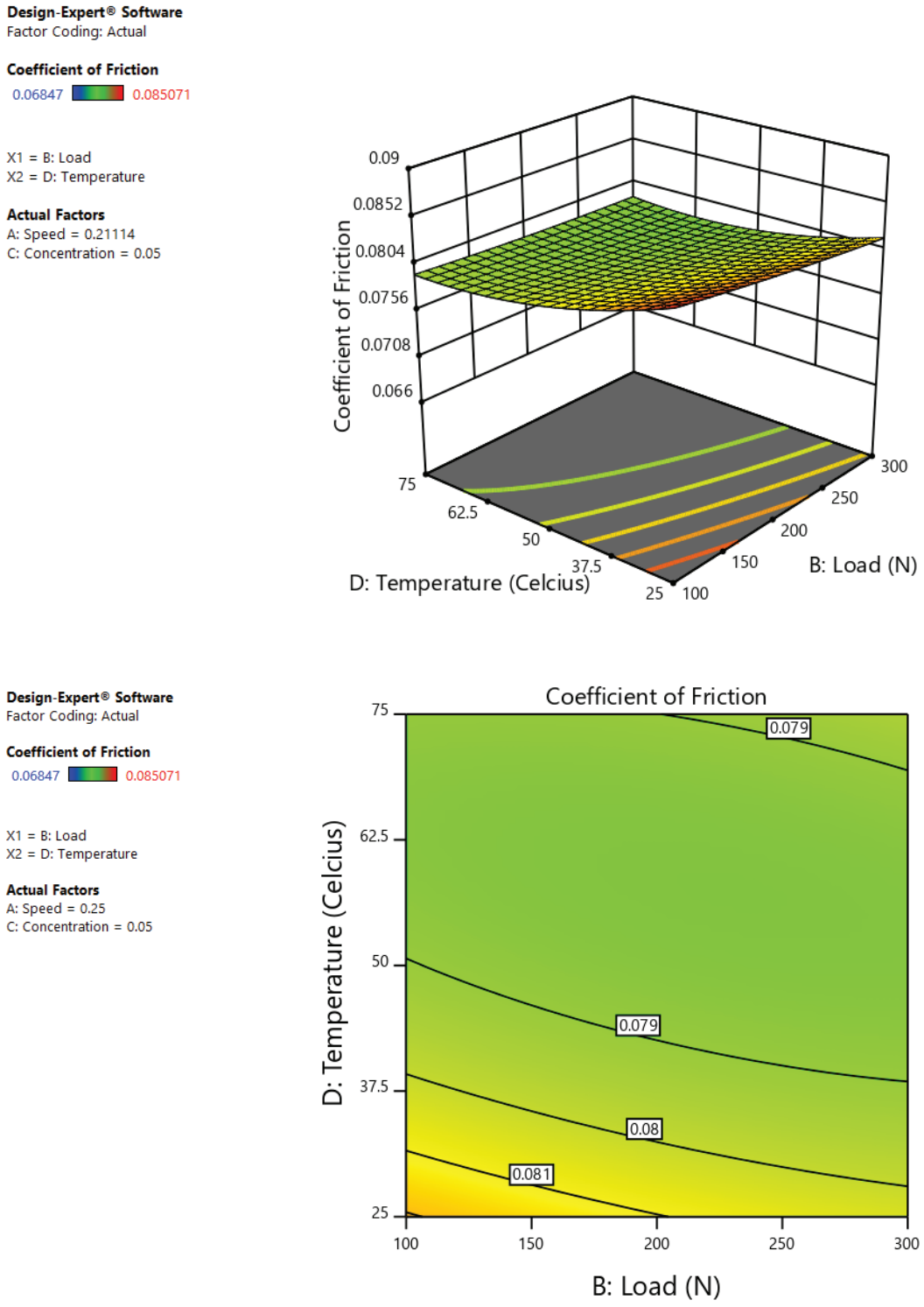

Figure 5.13 Load-temperature interaction 3D and contour plot

Rising temperatures reduce the film thickness by lowering oil viscosity, as shown in Figure 5.13. While temperature significantly affects COF, the impact of load is minimal. Increasing load expands the contact area, and nano-additives facilitate smoother particle movement within the contact region, effectively reducing COF. However, this interaction has minimal influence when the temperature is constant.

5.7.6. Concentration-temperature interaction

Figure 5.14 illustrates; higher concentrations of hybrid additives significantly reduce COF. This is due to improved dispersion of zinc oxide particles in the lubricant, stabilizing graphene sheets through functionalization. The rolling motion of zinc oxide particles and the low shear strength of graphene collectively reduce friction. However, temperature changes have a negligible effect on COF when other parameters are constant. The statistical analysis reveals that concentration is the most critical factor, with a p-value below 0.0001 confirming its significant influence on COF.

5.7.7. Concentration-speed interaction

A strong relationship exists between concentration and speed, as shown in Figure 5.15. At low speeds, increasing concentration noticeably reduces COF. This reduction becomes even more pronounced at higher speeds, where the film thickness improves lubrication. However, excessive particle interactions at the surface can limit the film's effectiveness. The study confirms that a 0.1 wt% concentration achieves the maximum COF reduction.

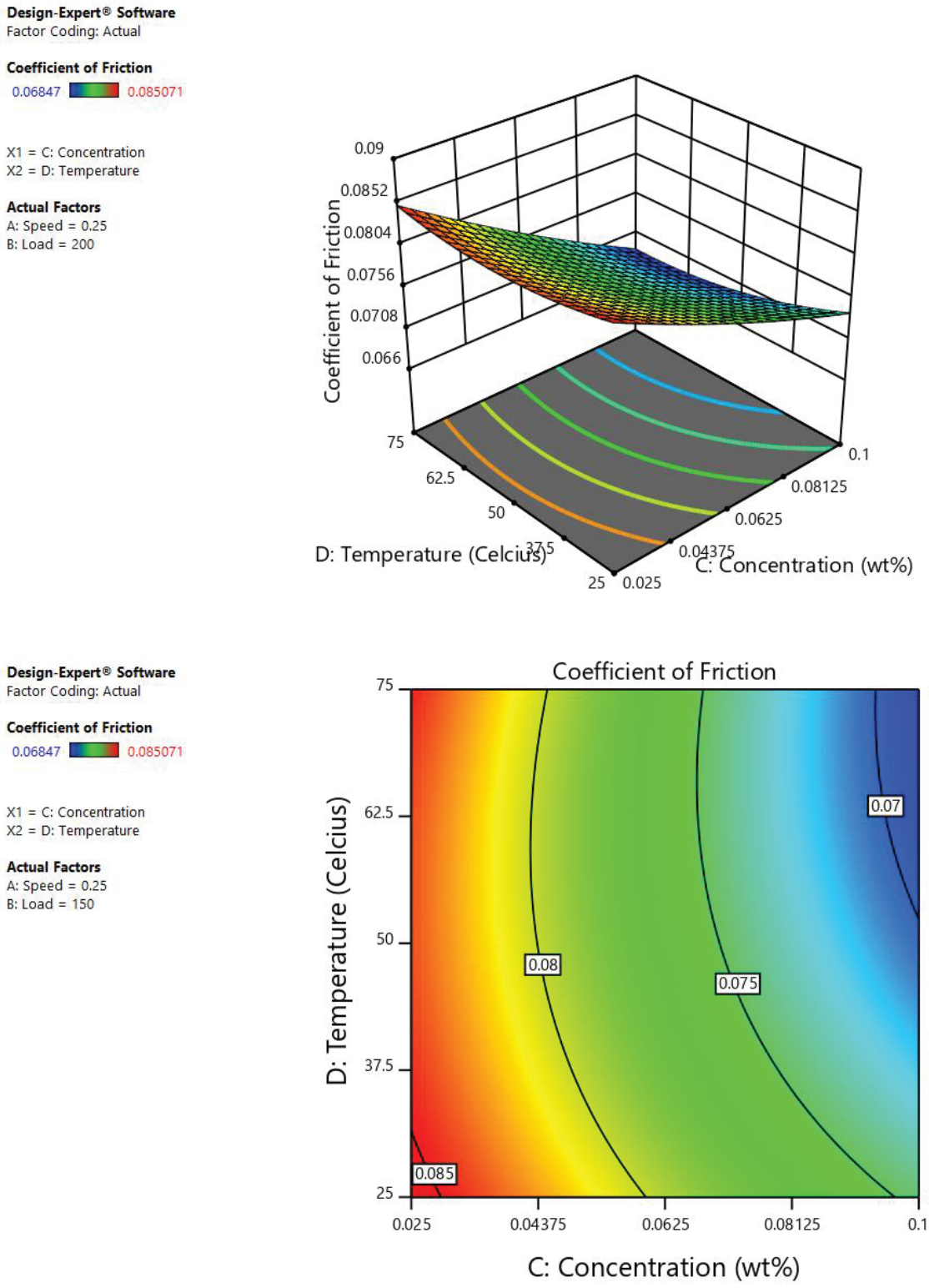

Figure 5.14 Concentration-temperature interaction 3D and contour plot

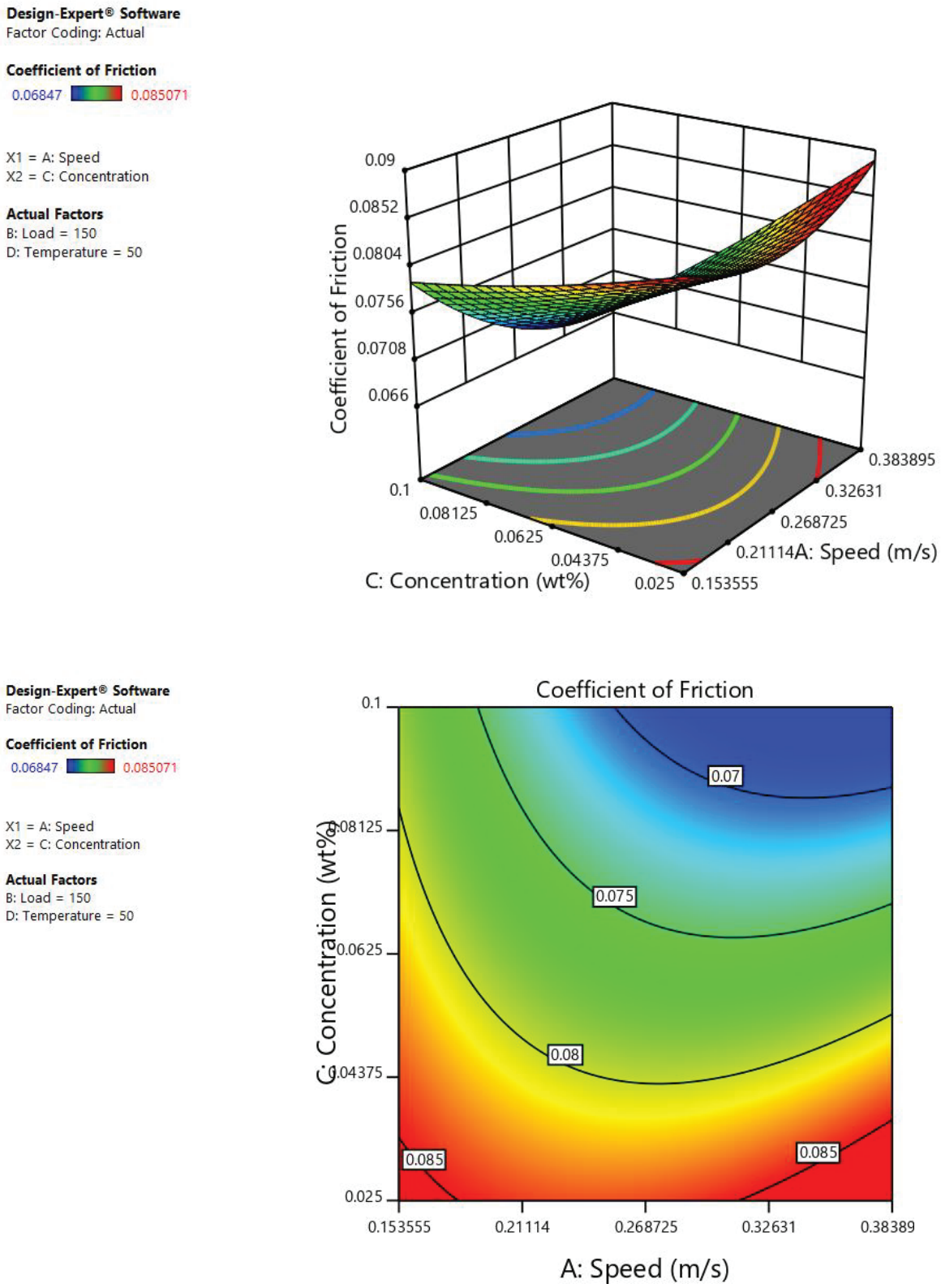

Figure 5.15 Concentration-speed interaction 3D and contour plot

5.7.8. Concentration-load interaction

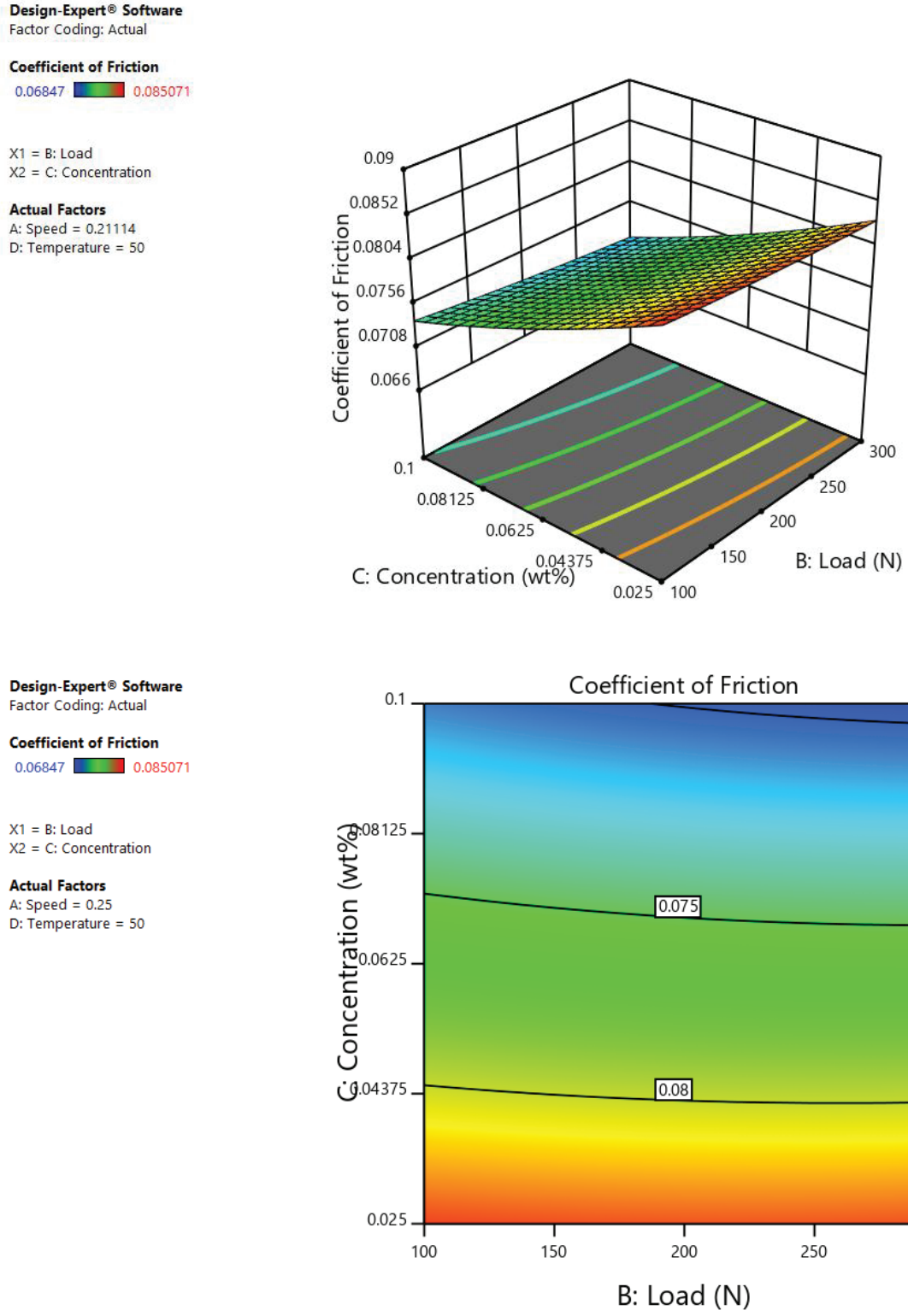

Figure 5.16 Concentration-load interaction 3D and contour plot

The interaction between load and concentration is relatively minor, as evidenced by the flat response curve in Figure 5.16. At higher concentrations, a slight reduction in COF is observed as the load increases. However, excessive concentrations may lead to agglomeration, diminishing lubricant performance. At 300 N, the maximum contact pressure promotes appropriate exfoliation of graphene layers, but further exfoliation effects are negligible due to prior ultrasonication.

5.7.9. Temperature-speed interaction

Figure 5.17 reveals that at lower speeds, increasing temperature slightly reduces COF due to improved lubrication in boundary regimes. However, at higher speeds, reduced viscosity leads to increased asperity contact, raising COF. These changes reflect the transition between lubrication regimes. At lower viscosities, stable film formation occurs easily, reducing COF. Conversely, in mixed regimes, increased asperity contacts lead to friction.

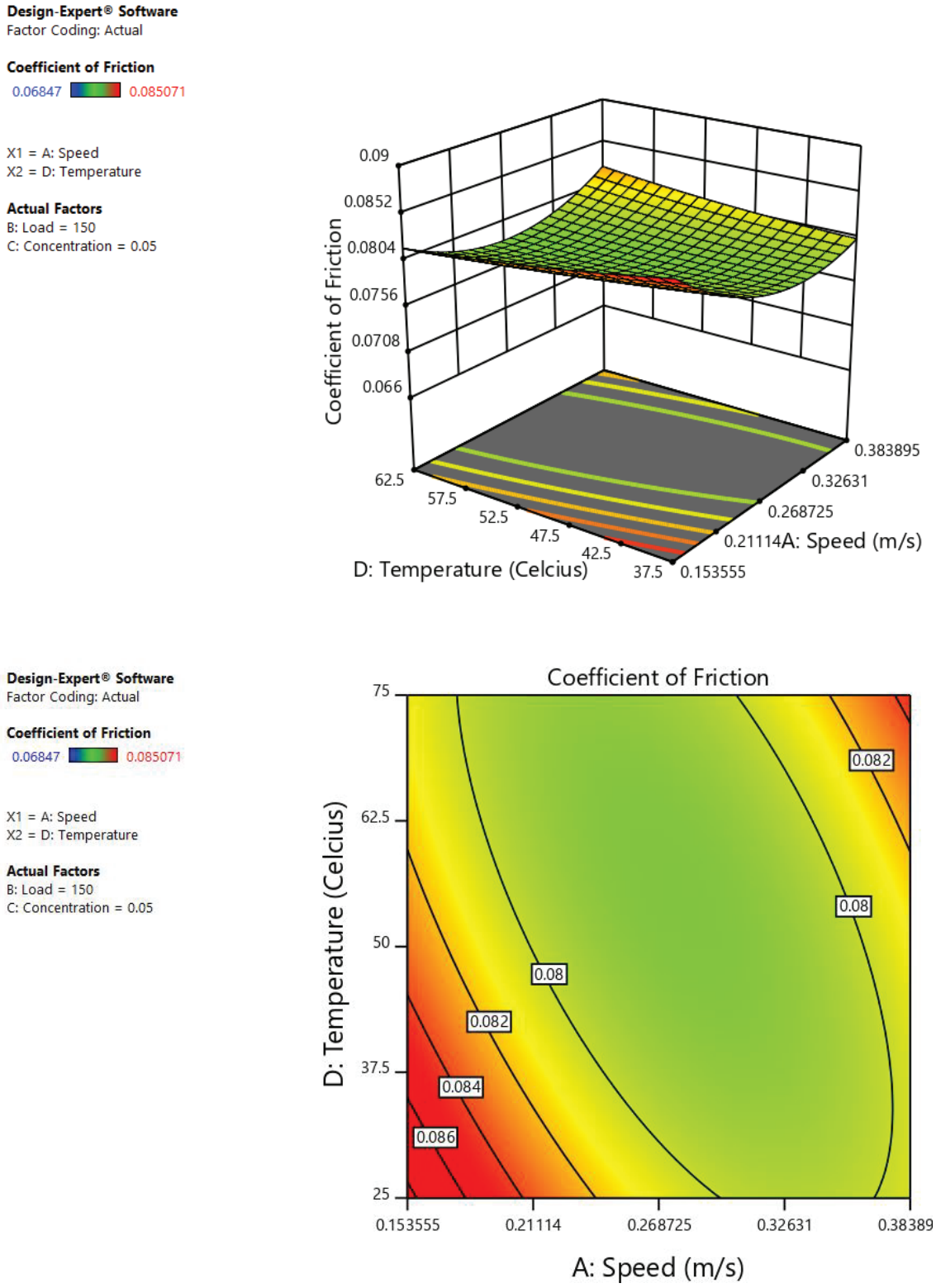

Figure 5.17 Temperature-speed interaction 3D and contour plot

The study highlights the complex interplay of factors influencing COF in hybrid nanolubricants. Speed and concentration emerge as the most influential parameters, while load and temperature have secondary effects. The statistical analysis confirms the robustness of the model, paving the way for further exploration of these interactions in tribological applications.

5.8. Mechanism of lubrication

The reduction in the coefficient of friction (COF) can be attributed to the unique roles played by the hybrid additives. The spherical ZnO particles create a rolling effect, which reduces friction between the contacting surfaces. Meanwhile, the presence of GO enhances this effect by facilitating smooth sliding between the surfaces, working synergistically with ZnO to minimize friction. GO nanosheets primarily act as a protective agent, forming a thin layer on the surface and reducing wear [110].

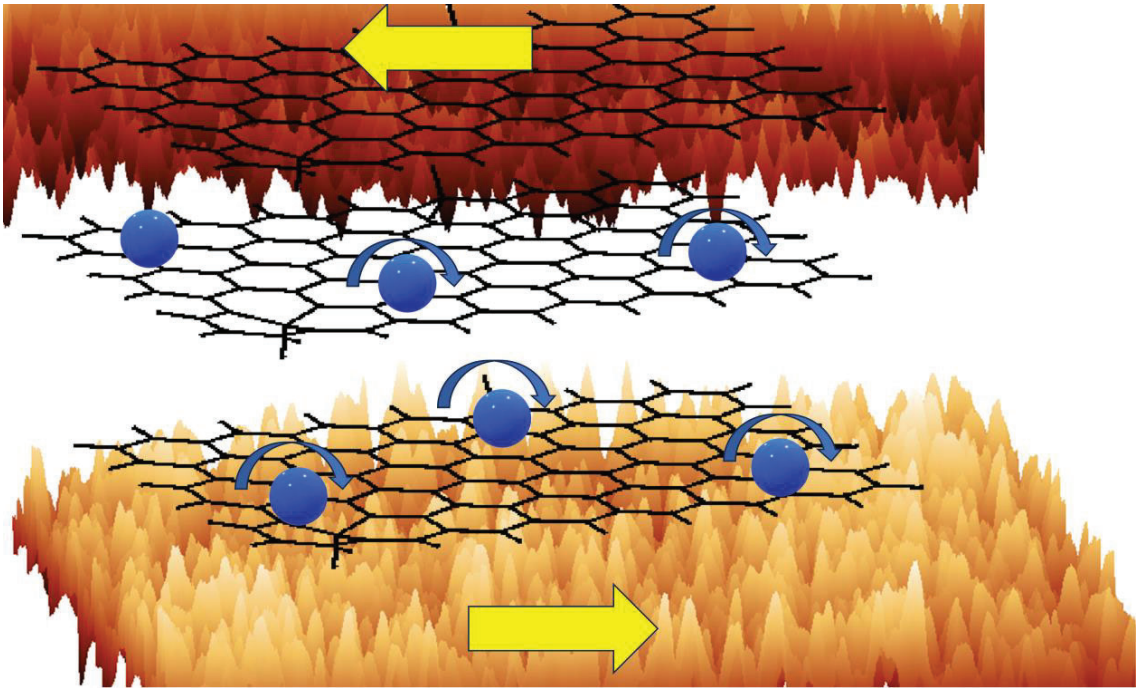

Figure 5.18 Schematic presentation of lubrication mechanism of AZnOGO nanolubricant

This synergistic behavior is evident in Figure 5.18, which shows the smallest wear scar at a ZnO-GO concentration of 0.0625 wt%. However, as the concentration increases beyond this point, the wear scar diameter grows. This can be explained by the abrasive nature of ZnO particles. ZnO, which is harder than GO on the Mohs scale, is more prone to scratching the surface. As a result, higher concentrations of ZnO lead to increased wear, outweighing the protective effect of GO.

5.9. Chapter summary

The study on the lubricating capabilities of the AZnOGO hybrid lubricant demonstrates the synergistic effects of spherical zinc oxide (ZnO) particles functionalized with graphene oxide (GO) in improving tribological performance. The statistical analysis and experimental results highlight the quadratic model as the most suitable for predicting the behavior of the hybrid lubricant, with high regression coefficients confirming the model's reliability in capturing the experimental outcomes. Among the various factors influencing the COF, the concentration of AZnOGO was found to be the most significant, followed by speed and temperature, while the load had the least impact within the studied range. The Response Surface Methodology (RSM) indicated that increasing the concentration of AZnOGO effectively reduces friction, although it is crucial to balance this increase to minimize material removal and wear. Further analysis revealed that a concentration of 0.0625 wt% provided the most effective wear prevention, with surface film formation offering a 48% improvement compared to a higher concentration of 0.1 wt%, where agglomeration led to diminished performance. Overall, the study underscores the potential of AZnOGO as a high-performance hybrid lubricant, where careful optimization of concentration and operational parameters can significantly enhance its friction-reducing and wear-preventing capabilities.